Topological Switch for Non-Hermitian Skin Effect in Cold-Atom Systems with Loss

Linhu Li,* Ching Hua Lee,† and Jiangbin Gong‡
Department of Physics, National University of Singapore, Singapore 117551, Republic of Singapore

(Received 21 October 2019; accepted 29 May 2020; published 22 June 2020)

We propose a realistic cold-atom quantum setting where topological localization induces nonreciprocal pumping. This is an intriguing non-Hermitian phenomenon that illustrates how topology, when assisted with atom loss, can act as a "switch" for the non-Hermitian skin effect (NHSE), rather than as a passive property that is modified by the NHSE. In particular, we present a lattice-shaking scenario to realize a two-dimensional cold-atom platform, where nonreciprocity is switched on only in the presence of both atom loss and topological localization due to time-reversal symmetry breaking. The resultant nonreciprocal pumping is manifested by asymmetric dynamical evolution, detectable by atomic populations along the system edges. Our setup may trigger possible applications in nonreciprocal atomtronics, where loss and topological mechanisms conspire to control atomic transport. Its quantum nature will also facilitate future studies on the interplay between non-Hermiticity and many-body physics.

DOI: 10.1103/PhysRevLett.124.250402

Introduction.—Cold atoms on optical lattices provide a highly promising platform for demonstrating interesting topological and many-body physics [1,2]. Recent advances in lattice-shaking technology have enabled unprecedented tuning of effective tunneling amplitudes, leading to pioneering observations of various exotic topological states [3–9]. Beyond realizing conventional static and Floquet topological phases [10–18], cold atoms in optical systems are also suitable quantum platforms for simulating higher-order topology [19–24] and non-Hermitian effects [25–28], two classes of phenomena of intense current interest. Indeed, non-Hermiticity can be experimentally implemented through optically induced depopulating losses [27], and be fine-tuned to exhibit non-Hermitian topological degeneracies like exceptional points [26,29–32], lines [33–41], and surfaces [42,43], all possessing rich geometric structure without Hermitian analogs [44–46].

In this Letter, we propose the cold-atom realization of a novel phenomenon where topological localization in one direction breaks the reciprocity of a two-dimensional (2D) lattice system in the presence of atom loss, leading to transverse nonreciprocal pumping. In contrast to much contemporary theoretical [47–58] and experimental [59–62] literature focusing on the *breakdown* of conventional bulk-boundary correspondences (BBCs) caused by the non-Hermitian skin effect (NHSE), i.e., eigenmode localization at the boundaries, our proposal illustrates how nontrivial topology can conversely *cause* nonreciprocal pumping, as illustrated in Fig. 1(e). The resultant topology-induced NHSE, with non-Hermiticity implemented via atom loss only, is marked by corner mode accumulation scaling extensively with the system length [63], fundamentally unlike higher-order topological corner modes, Hermitian or otherwise [24,64–67]. Our results provide a new application of topology in non-Hermitian systems and may stimulate further work on nonreciprocal atomtronics, exploiting both atom loss and topological mechanisms to control atomic transport. Relying on a *quantum* platform with tunable interactions, our proposal is also intrinsically poised for further exploration on how the NHSE interplays with many-body phenomena like Bose-Einstein condensation, fractionalization, charge density waves, and Mott physics.

Our setup consists of an optically shaken lattice accommodating cold atoms, designed such that lattice anisotropy and antiphase shaking conspire to yield nontrivial first-order topological edge modes. The required atom loss is introduced through selective depopulation, by exciting the atoms into an excited state with a resonant beam. Together with lattice shaking, this effectively generates nonreciprocity with two sublattices favoring opposite directions, which can hence be balanced by intersublattice couplings and yields net reciprocity. Nevertheless, this picture breaks down at the system's edge, because topological edge modes possess sublattice polarization, hence breaking this reciprocity, and NHSE occurs in the transverse direction. Therefore, we can switch on and off the NHSE through inducing topological phase transitions. The resultant NHSE is further identified via asymmetric dynamical evolution arising from the broken reciprocity.

2D optical lattice and model Hamiltonian.—Consider a Fermi gas in a two-frequency, periodically driven 2D superlattice formed by three directed optical standing waves, described by the following potential [Fig. 1(a)]:

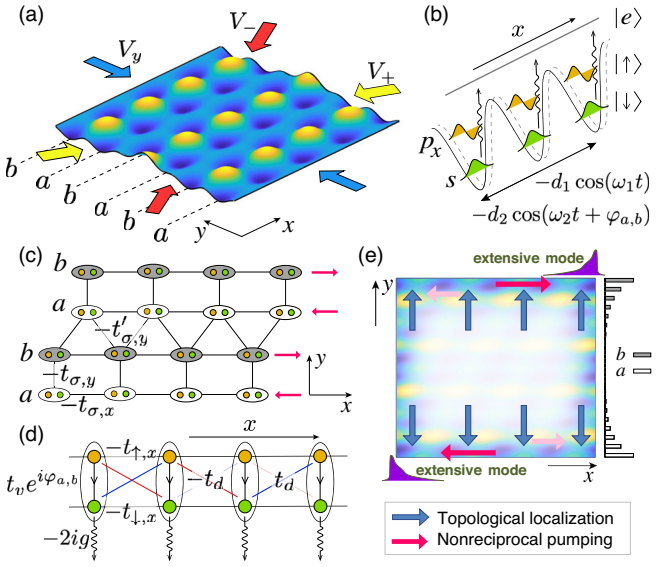

FIG. 1. (a) 2D optical lattice depicted by Eq. (1); dark blue color indicates minima of the potential, generating the a, b sublattices. (b) Effective 1D potential experienced by each sublattice along the x direction, with $|\uparrow\rangle$ and $|\downarrow\rangle$ representing the p_x and s orbitals. Atoms in the $|\downarrow\rangle$ state are resonantly excited to a third state $|e\rangle$, leading to loss. (c) The corresponding lattice structure of (a); pink arrows show the direction of nonreciprocity of each sublattice. (d) Two-leg system for each sublattice [white and gray rows in Fig. 1(c)], with yellow and green sites representing up and down pseudospins. (e) Mechanism for topology-induced nonreciprocal corner modes. The reciprocity is broken when topological boundary modes localize on the a (b) sublattices along the lower (upper) edge [white (gray) bars], such that nonreciprocal pumping toward the left (right) dominates.

$$V(x,y)=2V_y\left[\sin^2\left(\frac{2\pi}{\lambda_L}y\right)+\cos^2\left(\frac{4\pi}{\lambda_L}y\right)\right]+\sum_{s=\pm}2V_s(\omega_2 t)\cos^2\left[\frac{2\pi}{\lambda_L}\left([x-x_1(\omega_1 t)]-\frac{sy}{2}\right)+\frac{\pi}{4}\right], \tag{1}$$

with $d=\lambda_L/2$ the lattice constant along the y direction. V_y describes the strength of a static double-well potential realizable with two pairs of interfering laser beams [68–71]. Terms with coefficients $V_\pm$ represent additional potentials with time-modulated phases with frequency ω_1 and small amplitude modulation of frequency ω_2 through $V_\pm(\omega_2 t)=V_{xy}[1\pm A\cos(\omega_2 t+\varphi)]/2$. Because of this bichromatic driving [9], the positions of all the potential minima acquire time modulations $-d_1\cos(\omega_1 t)-d_2\cos(\omega_2 t+\varphi_{a,b})$, with $\varphi_a=\varphi_b+\pi=\varphi$ for sublattices a and b [72] [see Fig. 1(b)] and d_1 and d_2 explicitly given in Supplemental Material [72]. Further, we consider resonant frequency values $\omega_2=2\omega_1$ and $\hbar\omega_2$ close to the energy difference ε_{sp_x} between the s ($|\downarrow\rangle$) and p_x ($|\uparrow\rangle$) orbitals of the fermions, so that they can be coupled by a two-photon interorbital resonant couplings [9,75,76]. Non-Hermiticity is introduced by on site atom loss on the $|\downarrow\rangle$ state by using a resonant optical beam to transfer the atoms to an excited state $|e\rangle$ [Fig. 1(b)], with the loss rate controlled by the intensity of the resonant beam [27]. For other mechanisms causing two pseudospins to have different rates of loss, our description also applies upon adding an overall imaginary term to the spectrum (which leads to more decay in the dynamics). Finally, while our setup is valid for generic parameter values, we shall set $\lambda_L=532$ nm in the numerics that follow and consider small shaking amplitudes $d_2=d_1/20=\lambda_L/200$ [77].

In the high frequency regime with small oscillation amplitudes, the Magnus expansion approximation gives the effective *static* Hamiltonian $H(\boldsymbol{k})=\Psi^\dagger(\boldsymbol{k})h_{2D}(\boldsymbol{k})\Psi(\boldsymbol{k})$ with $\Psi^\dagger(\boldsymbol{k})=(\hat{a}^\dagger_{\uparrow\boldsymbol{k}},\hat{b}^\dagger_{\uparrow\boldsymbol{k}},\hat{a}^\dagger_{\downarrow\boldsymbol{k}},\hat{b}^\dagger_{\downarrow\boldsymbol{k}})$ creating states on a and b sublattices and $|\uparrow\rangle$ and $|\downarrow\rangle$ pseudospins, and [72]

$$h_{2D}(\boldsymbol{k})=h^+_\sigma(\boldsymbol{k})\sigma_0+h^-_\sigma(\boldsymbol{k})\sigma_3+h^+_\tau(\boldsymbol{k})\tau_0+h^-_\tau(\boldsymbol{k})\tau_3, \tag{2}$$

$$\begin{aligned}h^\pm_\sigma(\boldsymbol{k})&=-(2t_{\pm,x}\cos k_x-\Delta_\pm\pm ig)\tau_0\\&\quad-\{t_{\pm,y}+t'_{\pm,y}[\cos k_y+\cos(k_y-k_x)]\}\tau_1\\&\quad-t'_{\pm,y}[\sin k_y+\sin(k_y-k_x)]\tau_2,\\h^-_\tau(\boldsymbol{k})&=(t_v\cos\varphi)\sigma_1+(t_v\sin\varphi)\sigma_2,\\h^+_\tau(\boldsymbol{k})&=(2t_d\sin k_x)\sigma_2.\end{aligned} \tag{3}$$

Here τ_i and σ_i ($i=1,2,3$) are two sets of Pauli matrices acting on the sublattice and pseudospin spaces, respectively, with τ_0 and σ_0 their corresponding 2×2 identity matrices. The various coupling amplitudes t_v, t_d, $t_{\pm,\alpha}=(t_{\uparrow,\alpha}\pm t_{\downarrow,\alpha})/2$, and $t'_{\pm,\alpha}=(t'_{\uparrow,\alpha}\pm t'_{\downarrow,\alpha})/2$ arise from overlap integrals between lattice orbitals, as detailed in Supplemental Material [72]. This Hamiltonian can be visualized as the lattice in Fig. 1(c) with each $\tau\in\{a,b\}$ row represented by a two-leg lattice with couplings between s and p_x orbitals differing by a π phase, i.e., $\varphi_a=\varphi_b+\pi$ [Fig. 1(d)]. The shaking-induced interorbital coupling t_v and t_d breaks the time-reversal (TR) and inversion symmetries, respectively, giving rise to Chern topology [7]. Non-Hermiticity enters here through $-ig\tau_0(\sigma_0-\sigma_3)$, depicting a loss mechanism acting only on the $|\downarrow\rangle$ sector. Δ_- represents an energy offset between $|\uparrow\rangle$ and $|\downarrow\rangle$ sectors, and Δ_+ represents an overall energy shift that can be neglected. For concreteness, we have considered a lattice loaded with a fermionic gas of ^{173}Yb atoms following Refs. [8,9], although our scheme is also applicable for other cold atoms.

Edge modes from topological localization.—In the static ($\omega_1=\omega_2=0$) Hermitian limit, $h_{2D}(\boldsymbol{k})$ possesses sublattice symmetry and is topologically nontrivial with Z-quantized 1D Berry phase

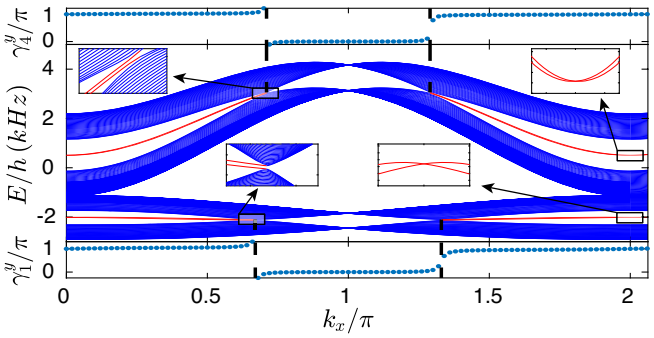

FIG. 2. x-PBC/y-OBC spectrum of h_{2D} without atom loss. Almost degenerate chiral edge modes (red curves) reflect the Chern topology, with their presence (or absence) at each k_x depending on whether the nearly quantized Berry phases γ_1^y and γ_4^y are close to π or zero. Effective parameters are $\varphi = \pi/2$ and $\{t_{+,x}, t_{-,x}, t_{+,y}, t_{-,y}, t'_{+,y}, t'_{-,y}, \Delta_-, t_d, t_v\} = \{0.38, 0.43, -0.11, -0.41, 0.44, 0.14, 2.07, -0.09, 0.16\}$ $h \times$ kHz, corresponding to the experimentally realistic parameters $V_{xy} = 3E_r = \frac{3}{2}V_y$ and $\omega_2 = 2\omega_1 = 10 \times 2\pi$ kHz, with $E_r = (\pi^2\hbar^2/2md^2) = h \times 4.1$ kHz.

$$\gamma_n^y(k_x) = -\mathrm{Im}\oint_0^{2\pi} dk_y \langle u_n(k_x, k_y)|\partial_{k_y}|u_n(k_x, k_y)\rangle \quad (4)$$

for each nth band $|u_n(k_x, k_y)\rangle$. When TR symmetry is broken through lattice shaking at nonzero $\omega_2 = 2\omega_1$ [72], its resultant topological boundary modes along the y edge cross over to Chern chiral edge modes, analogous to the zigzag edge modes of graphene or other honeycomb lattices under a circularly polarized laser [78–80]. As evident in Fig. 2 with open boundary conditions (OBCs) along y, these Chern edge states (red) are, however, only weakly separated due to the small shaking amplitudes and hence small interpseudospin coupling. This weak coupling also yields *almost quantized* Berry phases γ_1^y and γ_4^y shown in Fig. 2. The average Berry phase $\bar{\gamma}_n^y = \sum_{k_x} \gamma_n^y(k_x)/N_x$ used later gives the ratio of the total number of 1D edge modes to N_x under periodic boundary conditions (PBCs) along x and OBCs along y, which is proportional to the corner mode accumulation strength [63] and hence the consequent nonreciprocal pumping elaborated below.

Topology-induced nonreciprocal corner modes.—The non-Hermiticity introduced by on site atom loss does not merely induce a complex spectrum [Fig. 3(a)]. Interestingly, it also produces strong mode accumulation at two opposite corners, as conceptually sketched in Fig. 1(e) and quantitatively plotted in Fig. 3(b). Fundamentally unlike higher-order topological corner modes, our corner mode density scales *extensively* with the system length, as elucidated in Fig. 3(c) by the linear scaling behavior of the total mode intensity $\rho_{\mathrm{sum}}(x, y) = \sum_{n,\sigma} |\psi_n(\sigma, x, y)|^2$ with system length N_x at the nontrivial corner $(x, y) = (N_x, 1)$ [81]. Since the number of topological boundary modes is fixed by the topological invariant, this extensive scaling of mode intensity must be alternatively originated from some form of NHSE [82] realizing one form of hybrid corner modes [63] by exploiting atom loss.

To understand this enigmatic corner mode accumulation, first note that the loss term $-ig\tau_0(\sigma_0 - \sigma_3)$ in the $|\downarrow\rangle$ sector hardly changes the topological modes, as evident from comparing the Re$[E]$ inset of Fig. 3(a) with the dissipationless band structure in Fig. 2. With chosen experimental parameters producing considerably weak interorbital couplings t_v and t_d, one can also largely confine the damping effects within the $|\downarrow\rangle$ sector [orange in Fig. 3(a) with large -Im$[E]$], and observe nonreciprocal effects in the $|\uparrow\rangle$ sector possessing almost real eigenenergies.

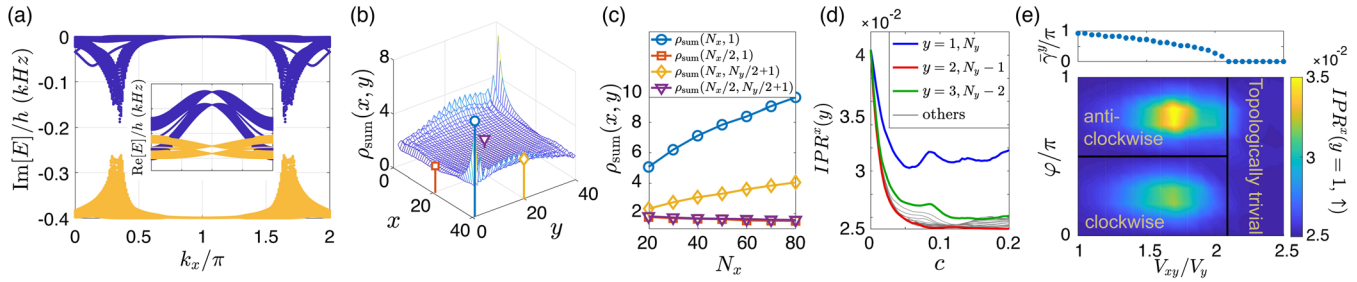

FIG. 3. (a) Imaginary and real parts of the x-PBC/y-OBC spectrum for nonzero loss $g = 0.2$ $h \times$ kHz, color indicating different bands. Other parameters follow Fig. 2, except for larger frequencies $\omega_2 = 2\omega_1 = 12 \times 2\pi$ kHz. (b) The corresponding summed eigenmode distribution $\rho_{\mathrm{sum}}(x, y)$, with corner mode densities $> \mathcal{O}(1)$, much greater than those of ordinary topological corner modes. (c) Scaling of $\rho_{\mathrm{sum}}(x, y)$ with system length N_x at various positions indicated in (b), with the NHSE giving rise to linear, i.e., extensive, scaling at the corner $(N_x, 1)$ (blue) and to a smaller extent along an edge $(N_x, N_y/2 + 1)$ (yellow), but not deep in the bulk at $(N_x/2, N_y/2 + 1)$ (purple) and the other edge at $(N_x/2, 1)$ (red). (d) The x direction IPR for different sublattices y as the intersublattice couplings $(t_{\sigma,y}, t'_{\sigma,y}) \to c(t_{\sigma,y}, t'_{\sigma,y})$ are suppressed, computed for $N_x = 40$. (e) Phase diagram showing anticlockwise (clockwise) topology-induced nonreciprocal pumping phases over a large range of optical lattice parameters φ and V_{xy}/V_y. The average Berry phase $\bar{\gamma}^y$ is nonzero in the topological phases, where the $\mathrm{IPR}^x_\uparrow$ for pseudo-spin-up component also peaks. The shaking frequency is set as $\omega_2 = 2\omega_1 = \epsilon_{sp_x}/\hbar$.

We can obtain intuition about how these nonreciprocal effects can be topology-induced from a gedanken experiment of tuning the couplings $(t_{\sigma,y}, t'_{\sigma,y}) \to c(t_{\sigma,y}, t'_{\sigma,y})$, where $c \in [0,1]$ interpolates between the decoupled limit and the full values of these couplings. In the fictitious $c = 0$ decoupled limit, the system is decoupled into a series of 1D two-leg ladders as in Fig. 1(d), with $\varphi_{a,b}$ differing by π between the sublattices a and b. Upon rotating the Pauli matrices, the on site loss term $ig\sigma_3$ becomes nonreciprocal couplings $ig\sigma_2$, and the decoupled 1D two-leg ladders resemble the non-Hermitian Su-Schrieffer-Heeger (SSH) model possessing the NHSE [47,72,83]. Hence, the two sublattices exhibit extensive skin mode accumulation at either the left ($x = 1$) or right ($x = N_x$) edge, with the same strength but opposite pumping directions when $\sin\varphi_a = -\sin\varphi_b$ (note that $\varphi_a - \varphi_b = \pi$) [72].

The *physical* spatial eigenmode distribution is obtained by restoring $t_{\sigma,y}$ and $t'_{\sigma,y}$, i.e., by tuning c from zero to one. This couples the two SSH-like sublattices, leading to destructive interference of the equal and opposite NHSEs. Since the $\tau = a, b$ sublattices of $h_{2D}(\boldsymbol{k})$ take similar forms, bulk modes are necessarily equitably distributed with little residual nonreciprocal pumping and, hence, mode accumulation. However, its topological modes along the top ($y = N_y$) and bottom ($y = 1$) are intrinsically sublattice polarized. Hence, the top- and bottommost rows of sites are expected to experience equal and opposite uncanceled NHSEs, leading to extensive mode accumulation at two of the four corners [Fig. 1(e)]. This mode accumulation within each sublattice row y can be quantified by the inverse participation ratio (IPR) in the x direction,

$$\mathrm{IPR}^x(y) = \sum_x \left[\frac{\sum_{\sigma,n}|\psi_n(\sigma,x,y)|^2}{\sum_x\sum_{\sigma,n}|\psi_n(\sigma,x,y)|^2}\right]^2, \qquad (5)$$

with $\psi_n(\sigma,x,y)$ the nth eigenstate, plotted against c for various rows y in Fig. 3(d). In particular, in the decoupled limit $c = 0$, $\mathrm{IPR}^x(y)$ is constant for different y, indicative of equally strong NHSE for each decoupled 1D two-leg ladder. As c increases to realistic values, the ladders couple, and $\mathrm{IPR}^x(y)$ rapidly decreases to the uniform limit $1/N_x$ in the bulk ($1 < y < N_y$), implying full delocalization along x. However, at the bottom (top) boundaries at $y = 1, N_y$ (blue curves), $\mathrm{IPR}^x(y)$ stabilizes at values much higher than $1/N_x$ as c increases, indicating left (right) mode accumulation which, in 2D, gives corner mode accumulation [Fig. 3(b)]. This nonreciprocal pumping can be also regarded as a strong manifestation of topological localization along y.

These observations are further digested in the phase diagram of Fig. 3(e). Intuitively, corner accumulation should be expected if 1D edge states exist in the nondissipative limit, e.g., whenever the average Berry phase $\bar{\gamma}^y \equiv \bar{\gamma}^y_4$ of the least dissipative (fourth) band is nonvanishing. In addition, Fig. 3(e) reveals that the corner mode localization, now quantified by the $\mathrm{IPR}^x_\uparrow$ of the $|\uparrow\rangle$ sector only (since the least dissipative band is almost $|\uparrow\rangle$ polarized), also varies strongly with optical lattice parameters φ and V_{xy}/V_y. Indeed, a weaker V_{xy} indicates stronger Hermitian couplings along the x direction, which effectively weakens the nonreciprocal pumping. Also, the NHSE completely disappears when $\varphi = 0$ or π [72]. Since $\bar{\gamma}^y = 0$ when $V_{xy}/V_y \gtrsim 2.1$ (i.e., no more edge states), most pronounced corner accumulation occurs at moderate V_{xy}/V_y and $\varphi = \pm\pi/2$, with the sign determining the chirality of the corner accumulation.

Dynamical behavior from nonreciprocal pumping.—While the IPR can measure the extent of induced localization, its purported nonreciprocal origin has to be verified through dynamical behavior. We compare the time evolution of initial states $\Psi^{L/R}_{\mathrm{ini}} = \sum_{x,y}\sum_{\sigma=\uparrow,\downarrow}\psi^{L/R}_{\mathrm{ini}}(\sigma,x,y)\,\hat{\tau}^\dagger_{\sigma,x,y}|0\rangle$ localized on the left and right corners, i.e., $\psi^L_{\mathrm{ini}}(\uparrow,1,N_y) = 1$ and $\psi^R_{\mathrm{ini}}(\uparrow,N_x,N_y) = 1$, respectively, with vanishing amplitudes for $|\downarrow\rangle$ and all other sites. The evolved states at time t are given by $\Psi^{L/R}_t = e^{-iHt/\hbar}\Psi^{L/R}_{\mathrm{ini}}$. The presence of topology-induced nonreciprocal pumping can be saliently observed in snapshots of $\Psi^{L/R}_t$ after a fixed time $t = t_0$. Figures 4(a)–4(d) illustrate the spatial densities $\rho^{L/R}_{t_0}(x,y) = \sum_\sigma|\psi^{L/R}_{t_0}(\sigma,x,y)|^2$, $\sigma = \uparrow,\downarrow$ for a representative $t_0 = 2$ ms, with Figs. 4(a) and 4(c)

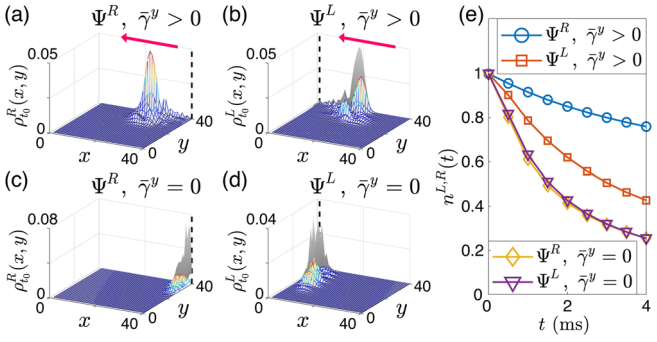

FIG. 4. (a)–(d) Population distribution snapshots of the states $\Psi^{L/R}_t$ after $t_0 = 2$ ms of evolution with $g = 0.5h \times$ kHz, as experimental signature of topology-induced corner accumulation. The initial state is prepared at (a),(c) $(\sigma, x_0, y_0) = (\uparrow, 1, N_y)$ and (b),(d) $(\uparrow, N_x, N_y)$, as indicated by the dashed lines. Pink arrows in (a),(b) indicate the direction of corner accumulation. For comparison, gray shadows indicate the same states evolving without dissipation. Other parameters are $\varphi = \pi/2$, $V_y = 2E_r$, and (a),(b) $V_{xy} = 3E_r$, $\omega_1 = 6$ kHz; (c),(d) $V_{xy} = 4.5E_r$, $\omega_1 = 9$ kHz. In (a), Ψ^R evolves almost identically as the no-loss case, hence covering the gray shadow. (e) Evolution of total population $n^{L/R}$ for cases (a)–(d) with different initial states and topology. Case (a), i.e., Ψ^R with $\bar{\gamma}^y > 0$ (blue circles), decays least, manifesting topology-induced nonreciprocal pumping.

showcasing $\rho^R_{t_0}$ and Figs. 4(b) and 4(d) showcasing $\rho^L_{t_0}$, as indicated by the vertical dashed lines. In the presence of topological edge modes localized primarily on one sublattice (i.e., $\bar{\gamma}^y \neq 0$), a state is subjected to asymmetric loss during its spreading. As illustrated in Figs. 4(a) and 4(b) for the case with right-to-left nonreciprocal pumping at $y = N_y$ row, Ψ^L_t [Fig. 4(b)] spreads from the left corner toward the right and is significantly more attenuated than Ψ^R_t [Fig. 4(a)] that is launched from the right. In contrast, when topological localization is absent [Figs. 4(c) and 4(d)], both Ψ^R_t and Ψ^L_t dissipate rapidly with time and do not propagate much along the boundaries, albeit having the same loss mechanism. Note that this asymmetric propagation is induced by NHSE switched on by topological localization and is not the chiral propagation of the Chern topology, which is extremely weak in our system. This asymmetry in dynamical propagation can be further quantified through the decaying of the population

$$n^{L/R}(t) = \sum_{x,y} \rho^{L/R}_t = \sum_{x,y} \sum_{\sigma} |\Psi^{L/R}_t(\sigma, x, y)|^2. \quad (6)$$

In Fig. 4(e), the initial state Ψ^R in the nontrivial ($\bar{\gamma}^y > 0$) phase, depicted by Fig. 4(a), indeed gets to decay the slowest. Both Ψ^R and Ψ^L in the nontopological cases [Figs. 4(c) and 4(d)] decay even faster than Ψ^L with $\bar{\gamma}^y > 0$.

Discussion.—To date, classical systems have been the main platforms to study NHSE, leaving the control of NHSE in tunable quantum systems still in its infancy. Via lattice shaking, we have proposed a versatile quantum platform where nontrivial topology, instead of being modified by non-Hermiticity, can *induce* nonreciprocal pumping when assisted by atom loss. Thus, NHSE can be turned on and off in a flexible and robust manner by tuning parameters to reach different topological phases, with no need to eliminate and reintroduce lossy mechanisms. While certain perturbations may also induce NHSE by generating unbalanced nonreciprocity, the latter will be sensitive to the perturbation details. By contrast, topological localization always induces an almost complete sublattice polarization along the boundaries, thus yielding robust nonreciprocal pumping.

Our large parameter space may afford further exploration into various active topical issues. As the effective two-leg ladders of each sublattice possess 1D Z-type topology, they also support topological edge localization along the x direction. The combination of both x and y localizations can lead to higher-order topological corner modes [84] in an extended parameter range [72]. With on site interactions induced by Feshbach resonances [85,86] or long-range interaction from dipolar Fermi gases, such as magnetic atoms [87,88], polar molecules [89–91], and Rydberg atoms [92,93], our proposed system also paves the way for exploring quantum many-body physics in the presence of non-Hermitian pumping, e.g., effective Bose-Einstein condensates for bosonic cold atoms and real-space Fermi surfaces [94] for fermions, as well as non-Hermitian fractional quantum Hall [95] and Mott insulators.

J. G. acknowledges support from the Singapore NRF Grant No. NRF-NRFI2017-04 (WBS No. R-144-000-378-281).

*phylli@nus.edu.sg
†phylch@nus.edu.sg
‡phygj@nus.edu.sg

[1] I. Bloch, J. Dalibard, and W. Zwerger, Many-body physics with ultracold gases, Rev. Mod. Phys. **80**, 885 (2008).
[2] N. Goldman, J. C. Budich, and P. Zoller, Topological quantum matter with ultracold gases in optical lattices, Nat. Phys. **12**, 639 (2016).
[3] H. Lignier, C. Sias, D. Ciampini, Y. Singh, A. Zenesini, O. Morsch, and E. Arimondo, Dynamical Control of Matter-Wave Tunneling in Periodic Potentials, Phys. Rev. Lett. **99**, 220403 (2007).
[4] J. Struck, C. Ölschläger, R. Le Targat, P. Soltan-Panahi, A. Eckardt, M. Lewenstein, P. Windpassinger, and K. Sengstock, Quantum simulation of frustrated classical magnetism in triangular optical lattices, Science **333**, 996 (2011).
[5] J. Struck, C. Ölschläger, M. Weinberg, P. Hauke, J. Simonet, A. Eckardt, M. Lewenstein, K. Sengstock, and P. Windpassinger, Tunable Gauge Potential for Neutral and Spinless Particles in Driven Optical Lattices, Phys. Rev. Lett. **108**, 225304 (2012).
[6] P. Hauke, O. Tieleman, A. Celi, C. Ölschläger, J. Simonet, J. Struck, M. Weinberg, P. Windpassinger, K. Sengstock, M. Lewenstein, and A. Eckardt, Non-Abelian Gauge Fields and Topological Insulators in Shaken Optical Lattices, Phys. Rev. Lett. **109**, 145301 (2012).
[7] G. Jotzu, M. Messer, R. Desbuquois, M. Lebrat, T. Uehlinger, D. Greif, and T. Esslinger, Experimental realization of the topological haldane model with ultracold fermions, Nature (London) **515**, 237 (2014).
[8] J. H. Kang, J. H. Han, and Y. Shin, Realization of a Cross-Linked Chiral Ladder with Neutral Fermions in a 1D Optical Lattice by Orbital-Momentum Coupling, Phys. Rev. Lett. **121**, 150403 (2018).
[9] J. H. Kang, J. H. Han, and Y. il Shin, Creutz ladder in a resonantly shaken 1D optical lattice, New J. Phys. **22**, 013023 (2020).
[10] N. Goldman, I. Satija, P. Nikolic, A. Bermudez, M. A. Martin-Delgado, M. Lewenstein, and I. B. Spielman, Realistic Time-Reversal Invariant Topological Insulators with Neutral Atoms, Phys. Rev. Lett. **105**, 255302 (2010).
[11] X.-J. Liu, K.-T. Law, T.-K. Ng, and P. A. Lee, Detecting Topological Phases in Cold Atoms, Phys. Rev. Lett. **111**, 120402 (2013).
[12] D. E. Liu, A. Levchenko, and H. U. Baranger, Floquet Majorana Fermions for Topological Qubits in Superconducting Devices and Cold-Atom Systems, Phys. Rev. Lett. **111**, 047002 (2013).
[13] X.-J. Liu, K. T. Law, and T. K. Ng, Realization of 2D Spin-Orbit Interaction and Exotic Topological Orders in Cold Atoms, Phys. Rev. Lett. **112**, 086401 (2014).

[14] I.-D. Potirniche, A. C. Potter, M. Schleier-Smith, A. Vishwanath, and N. Y. Yao, Floquet Symmetry-Protected Topological Phases in Cold-Atom Systems, Phys. Rev. Lett. **119**, 123601 (2017).

[15] L. Li, C. H. Lee, and J. Gong, Realistic Floquet Semimetal with Exotic Topological Linkages between Arbitrarily Many Nodal Loops, Phys. Rev. Lett. **121**, 036401 (2018).

[16] C. H. Lee, W. W. Ho, B. Yang, J. Gong, and Z. Papić, Floquet Mechanism for Non-Abelian Fractional Quantum Hall States, Phys. Rev. Lett. **121**, 237401 (2018).

[17] L. Zhou and J. Gong, Floquet topological phases in a spin-1/2 double kicked rotor, Phys. Rev. A **97**, 063603 (2018).

[18] Y.-B. Yang, L.-M. Duan, and Y. Xu, Dynamical Weyl points and 4D nodal rings in cold atomic gases, Phys. Rev. B **98**, 165128 (2018).

[19] W. A. Benalcazar, B. A. Bernevig, and T. L. Hughes, Quantized electric multipole insulators, Science **357**, 61 (2017).

[20] W. A. Benalcazar, B. A. Bernevig, and T. L. Hughes, Electric multipole moments, topological multipole moment pumping, and chiral hinge states in crystalline insulators, Phys. Rev. B **96**, 245115 (2017).

[21] F. Schindler, Z. Wang, M. G. Vergniory, A. M. Cook, A. Murani, S. Sengupta, A. Yu. Kasumov, R. Deblock, S. Jeon, I. Drozdov, H. Bouchiat, S. Guron, A. Yazdani, B. A. Bernevig, and T. Neupert, Higher-order topology in bismuth, Nat. Phys. **14**, 918 (2018).

[22] Z. Wang, B. J. Wieder, J. Li, B. Yan, and B. A. Bernevig, Higher-Order Topology, Monopole Nodal Lines, and the Origin of Large Fermi Arcs in Transition Metal Dichalcogenides $X\mathrm{Te}_2$ ($X = Mo$, W), Phys. Rev. Lett. **123**, 186401 (2019).

[23] C. Zeng, T. D. Stanescu, C. Zhang, V. W. Scarola, and S. Tewari, Majorana Corner Modes with Solitons in an Attractive Hubbard-Hofstadter Model of Cold Atom Optical Lattices, Phys. Rev. Lett. **123**, 060402 (2019).

[24] X.-W. L. C. Zhang, Higher-Order Topological Corner States Induced by Gain and Loss, Phys. Rev. Lett. **123**, 073601 (2019).

[25] C. M. B. S. Boettcher, Real Spectra in Non-Hermitian Hamiltonians Having PT Symmetry, Phys. Rev. Lett. **80**, 5243 (1998).

[26] I. Rotter, A non-Hermitian Hamilton operator and the physics of open quantum systems, J. Phys. A **42**, 153001 (2009).

[27] J. Li, A. K. Harter, J. Liu, L. de Melo, Y. N. Joglekar, and L. Luo, Observation of parity-time symmetry breaking transitions in a dissipative floquet system of ultracold atoms, Nat. Commun. **10**, 855 (2019).

[28] K. Yamamoto, M. Nakagawa, K. Adachi, K. Takasan, M. Ueda, and N. Kawakami, Theory of Non-Hermitian Fermionic Superfluidity with a Complex-Valued Interaction, Phys. Rev. Lett. **123**, 123601 (2019).

[29] M. V. Berry, Physics of non-Hermitian degeneracies, Czech. J. Phys. **54**, 1039 (2004).

[30] W. D. Heiss, The physics of exceptional points, J. Phys. A **45**, 444016 (2012).

[31] A. U. Hassan, B. Zhen, M. Soljačić, M. Khajavikhan, and D. N. Christodoulides, Dynamically Encircling Exceptional Points: Exact Evolution and Polarization State Conversion, Phys. Rev. Lett. **118**, 093002 (2017).

[32] W. Hu, H. Wang, P. P. Shum, and Y. D. Chong, Exceptional points in a non-Hermitian topological pump, Phys. Rev. B **95**, 184306 (2017).

[33] Y. Xu, S.-T. Wang, and L.-M. Duan, Weyl Exceptional Rings in a Three-Dimensional Dissipative Cold Atomic Gas, Phys. Rev. Lett. **118**, 045701 (2017).

[34] J. C. E. J. Bergholtz, Exceptional links and twisted fermi ribbons in non-Hermitian systems, Phys. Rev. A **98**, 042114 (2018).

[35] K. Moors, A. A. Zyuzin, A. Yu. Zyuzin, R. P. Tiwari, and T. L. Schmidt, Disorder-driven exceptional lines and fermi ribbons in tilted nodal-line semimetals, Phys. Rev. B **99**, 041116(R) (2019).

[36] H. Wang, J. Ruan, and H. Zhang, Non-Hermitian nodal-line semimetals with an anomalous bulk-boundary correspondence, Phys. Rev. B **99**, 075130 (2019).

[37] Z. Y. J. Hu, Non-Hermitian Hopf-link exceptional line semimetals, Phys. Rev. B **99**, 081102(R) (2019).

[38] J. Carlström, M. Stålhammar, J. C. Budich, and E. J. Bergholtz, Knotted non-Hermitian metals, Phys. Rev. B **99**, 161115(R) (2019).

[39] T. Yoshida, R. Peters, N. Kawakami, and Y. Hatsugai, Symmetry-protected exceptional rings in two-dimensional correlated systems with chiral symmetry, Phys. Rev. B **99**, 121101(R) (2019).

[40] K. Luo, J. Feng, Y. X. Zhao, and R. Yu, Nodal manifolds bounded by exceptional points on non-Hermitian honeycomb lattices and electrical-circuit realizations, arXiv:1810.09231v1.

[41] T. Yoshida and Y. Hatsugai, Exceptional rings protected by emergent symmetry for mechanical systems, Phys. Rev. B **100**, 054109 (2019).

[42] H. Zhou, J. Y. Lee, S. Liu, and B. Zhen, Exceptional surfaces in PT-symmetric non-Hermitian photonic systems, Optica **6**, 190 (2019).

[43] R. Okugawa and T. Yokoyama, Topological exceptional surfaces in non-Hermitian systems with parity-time and parity-particle-hole symmetries, Phys. Rev. B **99**, 041202(R) (2019).

[44] H. Shen, B. Zhen, and L. Fu, Topological Band Theory for Non-Hermitian Hamiltonians, Phys. Rev. Lett. **120**, 146402 (2018).

[45] C. Yin, H. Jiang, L. Li, R. Lü, and S. Chen, Geometrical meaning of winding number and its characterization of topological phases in one-dimensional chiral non-Hermitian systems, Phys. Rev. A **97**, 052115 (2018).

[46] L. Li, C. H. Lee, and J. Gong, Geometric characterization of non-Hermitian topological systems through the singularity ring in pseudospin vector space, Phys. Rev. B **100**, 075403 (2019).

[47] S. Y. Z. Wang, Edge States and Topological Invariants of Non-Hermitian Systems, Phys. Rev. Lett. **121**, 086803 (2018).

[48] S. Yao, F. Song, and Z. Wang, Non-Hermitian Chern Bands, Phys. Rev. Lett. **121**, 136802 (2018).

[49] F. K. Kunst, E. Edvardsson, J. C. Budich, and E. J. Bergholtz, Biorthogonal Bulk-Boundary Correspondence in Non-Hermitian Systems, Phys. Rev. Lett. **121**, 026808 (2018).

[50] Y. Xiong, Why does bulk boundary correspondence fail in some non-Hermitian topological models, J. Phys. Commun. **2**, 035043 (2018).

[51] L. J. Z. Song, Bulk-boundary correspondence in a non-Hermitian system in one dimension with chiral inversion symmetry, Phys. Rev. B **99**, 081103(R) (2019).

[52] C. H. L. R. Thomale, Anatomy of skin modes and topology in non-Hermitian systems, Phys. Rev. B **99**, 201103(R) (2019).

[53] C. H. Lee, G. Li, Y. Liu, T. Tai, R. Thomale, and X. Zhang, Tidal surface states as fingerprints of non-Hermitian nodal knot metals, arXiv:1812.02011.

[54] S. Longhi, Probing non-Hermitian skin effect and non-Bloch phase transitions, Phys. Rev. Res. **1**, 023013 (2019).

[55] S. Longhi, Topological Phase Transition in Non-Hermitian Quasicrystals, Phys. Rev. Lett. **122**, 237601 (2019).

[56] F. Song, S. Yao, and Z. Wang, Non-Hermitian Skin Effect and Chiral Damping in Open Quantum Systems, Phys. Rev. Lett. **123**, 170401 (2019).

[57] F. Song, S. Yao, and Z. Wang, Non-Hermitian Topological Invariants in Real Space, Phys. Rev. Lett. **123**, 246801 (2019).

[58] C. H. L. S. Longhi, Ultrafast and anharmonic Rabi oscillations between non-Bloch-bands, arXiv:2003.10763.

[59] T. Helbig, T. Hofmann, S. Imhof, M. Abdelghany, T. Kiessling, L. W. Molenkamp, C. H. Lee, A. Szameit, M. Greiter, and R. Thomale, Observation of bulk boundary correspondence breakdown in topolectrical circuits, arXiv:1907.11562v1.

[60] T. Hofmann, T. Helbig, F. Schindler, N. Salgo, M. Brzeziska, M. Greiter, T. Kiessling, D. Wolf, A. Vollhardt, A. Kabai, C. H. Lee, A. Bilui, R. Thomale, and T. Neupert, Reciprocal skin effect and its realization in a topolectrical circuit, arXiv:1908.02759v1.

[61] A. Ghatak, M. Brandenbourger, J. van Wezel, and C. Coulais, Observation of non-Hermitian topology and its bulk-edge correspondence, arXiv:1907.11619v1.

[62] L. Xiao, T. Deng, K. Wang, G. Zhu, Z. Wang, W. Yi, and P. Xue, Non-Hermitian bulk-boundary correspondence in quantum dynamics, Nat. Phys., 2020, https://doi.org/10.1038/s41567-020-0836-6.

[63] C. H. Lee, L. Li, and J. Gong, Hybrid Higher-Order Skin-Topological Modes in Nonreciprocal Systems, Phys. Rev. Lett. **123**, 016805 (2019).

[64] T. Liu, Y.-R. Zhang, Q. Ai, Z. Gong, K. Kawabata, M. Ueda, and F. Nori, Second-Order Topological Phases in Non-Hermitian Systems, Phys. Rev. Lett. **122**, 076801 (2019).

[65] E. Edvardsson, F. K. Kunst, and E. J. Bergholtz, Non-Hermitian extensions of higher-order topological phases and their biorthogonal bulk-boundary correspondence, Phys. Rev. B **99**, 081302(R) (2019).

[66] M. Ezawa, Electric-circuit realization of non-Hermitian higher-order topological systems, arXiv:1810.04527v1.

[67] Y. Liu, Y. Wang, N. C. Hu, J. Yu Lin, C. H. Lee, and X. Zhang, Topological corner modes in a brick lattice with nonsymmorphic symmetry, arXiv:1812.11846.

[68] S. Peil, J. V. Porto, B. L. Tolra, J. M. Obrecht, B. E. King, M. Subbotin, S. L. Rolston, and W. D. Phillips, Patterned loading of a Bose-Einstein condensate into an optical lattice, Phys. Rev. A **67**, 051603(R) (2003).

[69] S. Fölling, S. Trotzky, P. Cheinet, M. Feld, R. Saers, A. Widera, T. Müller, and I. Bloch, Direct observation of second-order atom tunnelling, Nature (London) **448**, 1029 (2007).

[70] S. Trotzky, P. Cheinet, S. Fölling, M. Feld, U. Schnorrberger, A. M. Rey, A. Polkovnikov, E. A. Demler, M. D. Lukin, and I. Bloch, Time-resolved observation and control of superexchange interactions with ultracold atoms in optical lattices, Science **319**, 295 (2008).

[71] M. Atala, M. Aidelsburger, J. T. Barreiro, D. Abanin, T. Kitagawa, E. Demler, and I. Bloch, Direct measurement of the Zak phase in topological Bloch bands, Nat. Phys. **9**, 795 (2013).

[72] See Supplemental Material at http://link.aps.org/supplemental/10.1103/PhysRevLett.124.250402, which includes Refs. [73,74], for more details about derivation of the tight-binding model, edge states with different interorbital couplings, the 1D two-leg ladder in the decoupled limit, nonreciprocal pumping in the bulk, dynamical evolution, and second-order topological phases of our model.

[73] F. Mei, J.-B. You, D.-W. Zhang, X. C. Yang, R. Fazio, S.-L. Zhu, and L. C. Kwek, Topological insulator and particle pumping in a one-dimensional shaken optical lattice, Phys. Rev. A **90**, 063638 (2014).

[74] N. Gemelke, E. Sarajlic, Y. Bidel, S. Hong, and S. Chu, Parametric Amplification of Matter Waves in Periodically Translated Optical Lattices, Phys. Rev. Lett. **95**, 170404 (2005).

[75] W. Z. H. Zhai, Floquet topological states in shaking optical lattices, Phys. Rev. A **89**, 061603(R) (2014).

[76] S.-L. Z. Q. Zhou, Shaping topological properties of the band structures in a shaken optical lattice, Phys. Rev. A **90**, 051601(R) (2014).

[77] Larger amplitudes lead to a greater number of nontrivial couplings without necessarily introducing new physics.

[78] G. Usaj, P. M. Perez-Piskunow, L. E. F. F. Torres, and C. A. Balseiro, Irradiated graphene as a tunable Floquet topological insulator, Phys. Rev. B **90**, 115423 (2014).

[79] P. M. Perez-Piskunow, G. Usaj, C. A. Balseiro, and L. E. F. . Torres, Floquet chiral edge states in graphene, Phys. Rev. B **89**, 121401(R) (2014).

[80] M. A. Sentef, M. Claassen, A. F. Kemper, B. Moritz, T. Oka, J. K. Freericks, and T. P. Devereaux, Theory of Floquet band formation and local pseudospin textures in pump-probe photoemission of graphene, Nat. Commun. **6**, 7047 (2015).

[81] The intensity at $(x, y) = (N_x, N_y/2 + 1)$ indicates a weak NHSE in the bulk, which can be removed with stronger y couplings [72].

[82] The NHSE is characterized by extensive mode accumulation along a boundary in the simultaneous presence of nonreciprocity and non-Hermiticity.

[83] W. P. Su, J. R. Schrieffer, and A. J. Heeger, Solitons in Polyacetylene, Phys. Rev. Lett. **42**, 1698 (1979).

[84] L. Li, M. Umer, and J. Gong, Direct prediction of corner state configurations from edge winding numbers in two- and three-dimensional chiral-symmetric lattice systems, Phys. Rev. B **98**, 205422 (2018).

[85] M. A. Cazalilla, R. Citro, T. Giamarchi, E. Orignac, and M. Rigol, One dimensional bosons: From condensed matter systems to ultracold gases, Rev. Mod. Phys. **83**, 1405 (2011).

[86] X.-W. Guan, M. T. Batchelor, and C. Lee, Fermi gases in one dimension: From Bethe ansatz to experiments, Rev. Mod. Phys. **85**, 1633 (2013).

[87] M. Lu, N. Q. Burdick, and B. L. Lev, Quantum Degenerate Dipolar Fermi Gas, Phys. Rev. Lett. **108**, 215301 (2012).

[88] K. Aikawa, A. Frisch, M. Mark, S. Baier, R. Grimm, and F. Ferlaino, Reaching Fermi Degeneracy Via Universal Dipolar Scattering, Phys. Rev. Lett. **112**, 010404 (2014).

[89] L. De Marco, G. Valtolina, K. Matsuda, W. G. Tobias, J. P. Covey, and J. Ye, A degenerate Fermi gas of polar molecules, Science **363**, 853 (2019).

[90] K.-K. Ni, S. Ospelkaus, M. H. G. De Miranda, A. Pe'Er, B. Neyenhuis, J. J. Zirbel, S. Kotochigova, P. S. Julienne, D. S. Jin, and J. Ye, A high phase-space-density gas of polar molecules, Science **322**, 231 (2008).

[91] S. Ospelkaus, A. PeEr, K.-K. Ni, J. J. Zirbel, B. Neyenhuis, S. Kotochigova, P. S. Julienne, J. Ye, and D. S. Jin, Efficient state transfer in an ultracold dense gas of heteronuclear molecules, Nat. Phys. **4**, 622 (2008).

[92] M. Saffman, T. G. Walker, and K. Mølmer, Quantum information with Rydberg atoms, Rev. Mod. Phys. **82**, 2313 (2010).

[93] A. B. T. Lahaye, *Interacting Cold Rydberg Atoms: A Toy Many-Body System* (Birkhuser, Cham, 2016), Vol. 68.

[94] S. Mu, C. H. Lee, L. Li, and J. Gong, Emergent Fermi surface in a many-body non-Hermitian fermionic chain, arXiv:1911.00023v1.

[95] T. Yoshida, K. Kudo, and Y. Hatsugai, Non-Hermitian fractional quantum Hall states, Sci. Rep. **9**, 1 (2019).